energies

*Article*

# Hybrid Model of Rolling-Element Bearing Vibration Signal

**Adam Jablonski**

Department of Robotics and Mechatronics, Faculty of Mechanical Engineering and Robotics, AGH University of Science and Technology, 30-059 Krakow, Poland; ajab@agh.edu.pl

**Abstract:** The generation of synthetic vibration signals enables the testing of novel machine diagnostic methods without the costly introduction of real failures. One of major goals of vibration-based condition monitoring is the early detection of bearing faults. This paper presents a novel modeling technique based on the combination of the known mechanical properties of a modeled object (phenomenological part) and observation of a real object (behavioral part). The model uses the real pulse response of bearing housing, along with the external instantaneous machine speed profile. The presented method is object-oriented, so it is applicable to a large group of machinery.

**Keywords:** rolling-element bearing modelling; cyclo-non-stationary signal; bearing diagnostics; envelope analysis; resampling

check for updates

**Citation:** Jablonski, A. Hybrid Model of Rolling-Element Bearing Vibration Signal. *Energies* **2022**, *15*, 4819. https://doi.org/10.3390/en15134819

Academic Editor: Paolo Mercorelli

Received: 30 May 2022
Accepted: 29 June 2022
Published: 30 June 2022



## 1. Introduction

Models of machine failures enable the generation of data used for the training of various data analysis systems [1], which play important roles in maintenance scheduling. This training generally covers data pre-processing, feature selection, and data analysis. Generating synthetic data is far cheaper, faster, and more convenient than collecting real data from individual machine failures. Such models of machine damage are typically constructed on the basis of the physical nature of the damage [2,3] (physical models), or on the basis of data generated by the object, so-called data-driven models [4,5]. Theoretically, the physical model should generate data corresponding to any possible machine damage; however, they are burdened with a relatively high level of approximations and assumptions. Additionally, any real material variations (such as manufacturing variations) or operational variations must be modeled separately, resulting in a large set of model variables. Data-driven models, on the other hand, are inherently associated with true operational conditions of machinery, but their range of fault representation (e.g., failure mode, size of the damage, fault severity) is limited to the current true machine state and is, therefore, burdened with undetermined uncertainty beyond it. An interesting approach to rolling-element bearing (REB) signal modelling is given in [6], where the authors claim that lack of data on failure models within data-driven models could be solved by data fusion techniques. The authors propose to combine a complete dataset representing a machine healthy state with synthetically generated failure mode data. As shown, this approach could provide the data necessary to train models in a wide variety of failure classifications. Nevertheless, the failure mode data used in multi-body techniques and data-driven techniques (namely, neural networks (NN) and support vector machines (SVM)) are in favor within feature extractions, classification, diagnostics, and analysis of remaining useful life (RUL).

The basic impulsive character of faulty rolling-element bearing is addressed in, among others, [7], as well as by McFadden and Smith [8,9]. The following research examines the influence of manufacturing errors of fault signature [10], and the effect of instantaneous load and speed with respect to rolling-element bearing defect size [11]. A comparative study of a simulated physical model with a finite-element model of faulty REB is presented in [12]. Recently, Wrzochal and Adamczyk [13] provide a detailed mathematical study on different REB modeling techniques, namely, the basic model with four degrees of freedom, a model with changing defect topography, a model with outer ring deformation, a model with waviness of rings, and, finally, a dynamic model with a variable viscosity damping coefficient. In their study, they tackle the problem of modeling simultaneous deformations within the ball–raceway contact zone, lubrication, friction process, and the geometrical structure of working surfaces. As concluded in [14–17], some of these problems, considered analytically in [13] might be solved by the numerical techniques shown in [18], especially regarding the modeling of dynamic conditions originating from different manufacturing, operational conditions, and assembly imperfections. Two year later, Borghesani et al. supplemented analytical REB models with analytical consideration in an assessment of true- vs. pseudo-cyclostationarity in REB signals [19].

The current paper proposes a hybrid model, which combines phenomenological features of an REB-induced vibration signal with its behavioral features. This model partially takes advantage of the analytical consideration presented in [20], where the REB signal model for constant speed presented in Equation (1) is extended to a more general, transient state, presented in Equation (2):

$$x(\theta) = \sum_{i=-inf}^{+inf} A_i \mathrm{s}(\theta - \mathrm{i}\Theta - \Psi_i) + \mathrm{n}(\theta) \tag{1}$$

$$x(t) = \sum_{i=-inf}^{+inf} A_i \mathrm{s}(\mathrm{t} - T_i) + \mathrm{n}(\mathrm{t}) \; with \; T_i = \sum_{k=1}^{i} \frac{\Theta}{\overline{\omega_k}} + \Psi_i \tag{2}$$

where $\overline{\omega_k}$ represents average machine speed between $(k-1)$-th vs. $k$-th REB impact, $\Theta$ is the average angular period of pulses, $n(t)$ is the environmental noise represented by a repetition of the impulse response of the structure $s(t)$, triggered, and A-modulated by subsequent REB impacts. The standard variable T represents expected period time, while $\Psi$ represents jitter (in both time and angle domains). As shown in the paper, the accepted scenario eventually follows the concept of the reversed squared envelope spectrum presented in [20], as it enables the generation of distinctive envelope components for REB vibration signals under simultaneous variable speed regime and jitter. While [20] discusses the general difference in true bearing characteristic frequencies and analytical values with respect to transient states, the current paper discusses the influence of the speed profile generation method on the smearing of the envelope spectrum in the order domain.

The paper is organized as follows: Section 2 shows a step-by-step construction of a generalized synthetic vibration signal from a real single pulse to the entire model. Section 3 illustrates the frequency and envelope analysis of the generated signal.

## 2. Signal Generation Methodology

### 2.1. Overview

The presented method enables the simulation of rotary machine faults under non-stationary conditions. In this paper, a local fault of a rolling-element bearing is considered. Formally, the presented model could be classified as a hybrid parametric model, because it combines the parametric phenomenological model with the parametric behavioral model.

The first part of the model—the phenomenological part—in contrast to the physical nature of failure modes used in some models [2,3], does not operate on primary object properties (mass, damping, and stiffness), but takes advantage of failure signal patterns, which are associated with particular failure modes. These patterns are based on the kinetostatic analysis of a particular drive train, as well as on well-accepted knowledge on vibration analysis and failure modes [21].

The second part of the model—the behavioral part—is, in a sense, a data-driven method, but modified. In this part, the real signal recorded from a machine of interest is used to determine characteristics of random structural vibrations for failure simulation. In this way, experimental observation of the behavior of the machine is used to approximate the real signal. As this observation is made without precise apparatus, which give detailed information about root processes (just a simple measurement of system response is required), this part of the model is classified as a behavioral part. The scope of observations considered in the presented model includes instantaneous speed characteristics, REB slip, amplitude–frequency characteristics of structural vibrations, phase–frequency characteristics of structural vibrations, and generalized amplitude and frequency modulations of 2nd order cyclostationary components [22], extended to a cyclo-non-stationary regime [23].

Figure 1 illustrates the general methodology of the generation of a hybrid vibration signal simulating a REB fault. The proposed method has three general stages. In the first stage, a real vibration pulse is collected from the mechanical object of interest. In stage 2, this signal is used to generate a set of pulses, which occur at pre-calculated timestamps. Finally, the amplitude of individual pulses is scaled according to the real amplitude–frequency characteristics of the object as a function of instantaneous machine speed. In this way, the synthetic signal enables the generation of a faulty REB signal, without an actual REB fault. Sections 2.2–2.4 describe the consecutive steps of the methodology in detail.

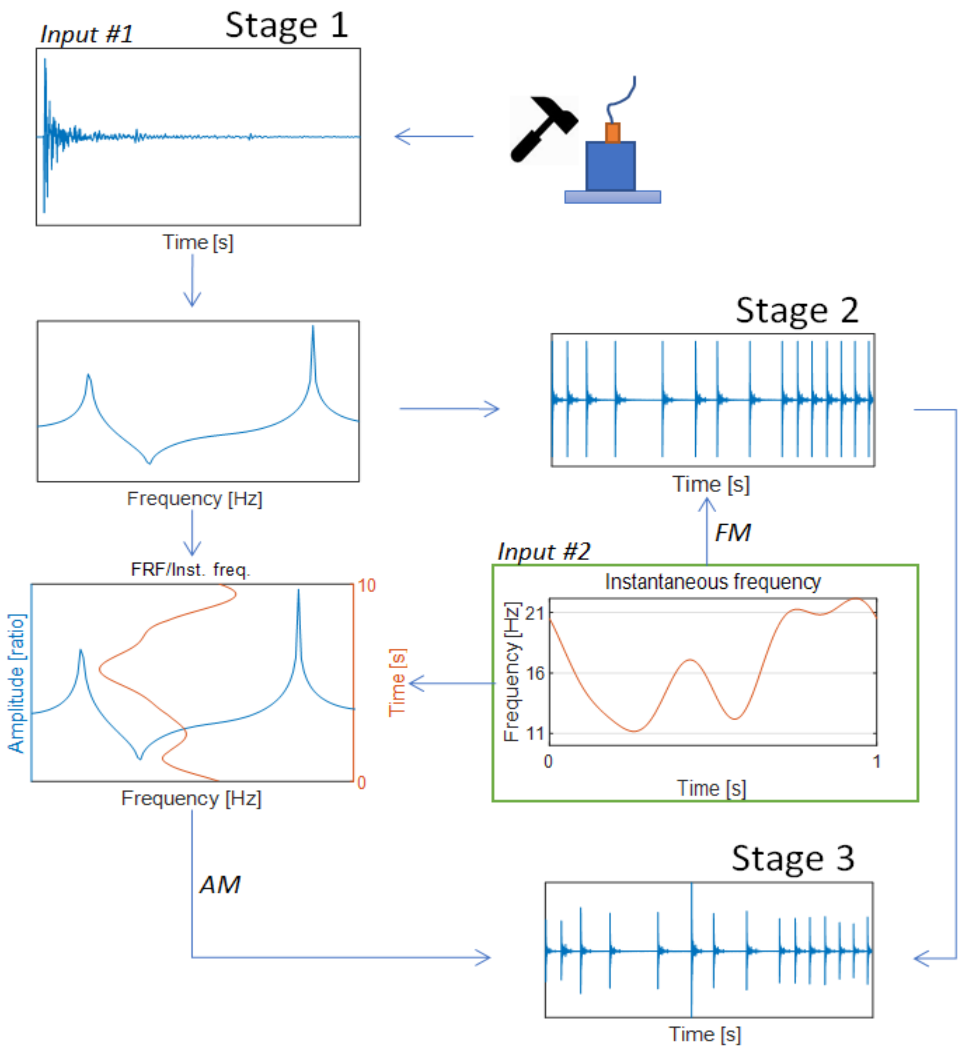


**Figure 1.** Methodology of generation of REB signal.

*2.2. Base Pulse*

First, the housing of the REB of interest needs to be provided, as illustrated in Figure 2. With the use of some kind of metal object, vibrations of the housing were induced. This response is similar to a system response generated by a faulty bearing, but this action does not require the bearing to be faulty. During the experiment, a standard bearing housing on the AVM test bench was selected.

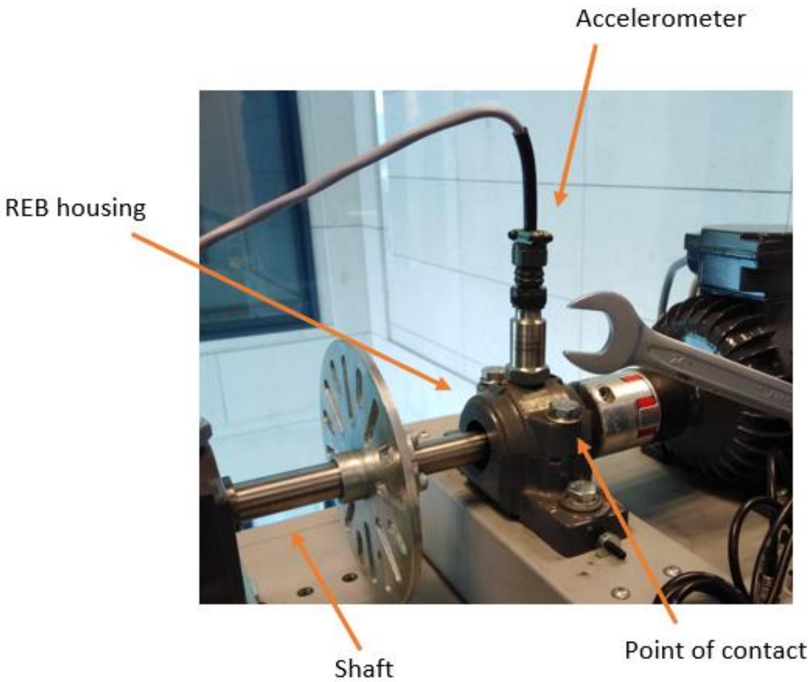


**Figure 2.** REB housing.

This operation was repeated multiple times. As illustrated in Figure 3, in practice, some pulses generate saturation of acquisition path, while others use a relatively small channel range. From a set of pulses, a single pulse is selected, as illustrated in Figure 4. This repetition enables the selection of such a pulse, which covers a majority of the physical channel range, yet it does not saturate it. In the selected example, the pulse covers over 90% of the physical input range of a 24-bit ADC (analog-to-digital) converter.

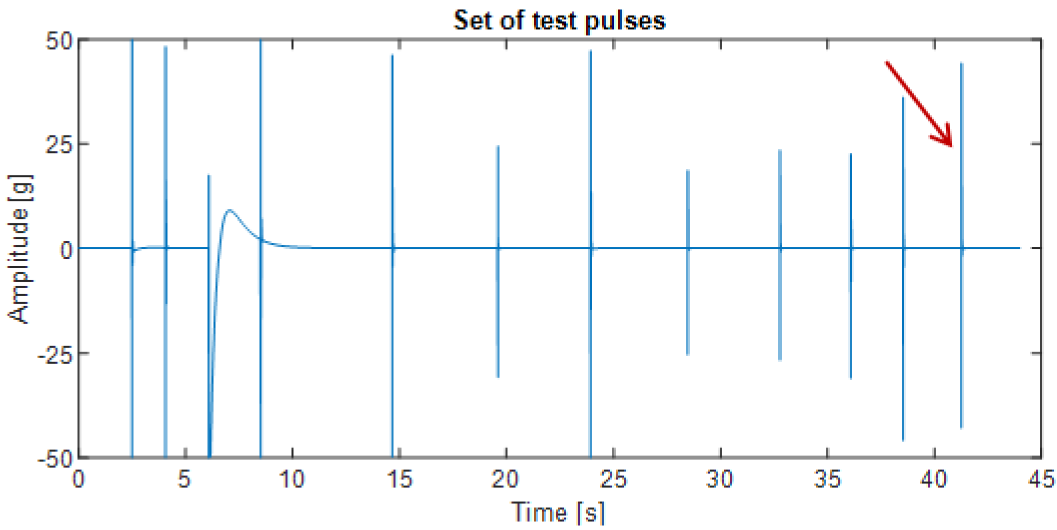


**Figure 3.** Selection of suitable pulse. The arrow indicates selected pulse.

Figure 4 shows a time plot of the pulse. As visually assessed, the full damping of the pulse lasts ca. 0.5 s. The next question is how much could it be shortened to still represent structural vibrations of the investigated object and be sufficient for signal generation. This shortening determines boundary condition of the proposed algorithm.

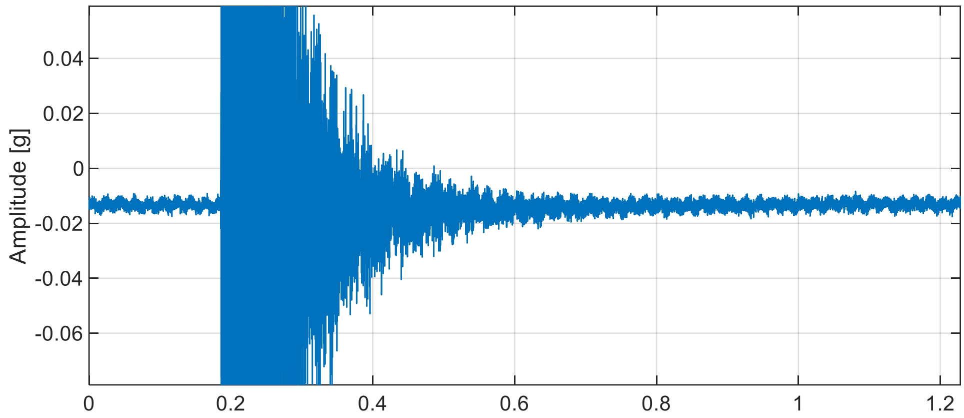


**Figure 4.** Approximation of pulse damping time.

Figure 5 illustrates four versions of this pulse: 0.5 s (full length), 0.2 s, 0.05 s, and 0.01 s. Individual pulses are presented in the same figure. Listed duration times correspond to REB characteristic frequencies from 1 Hz up to 100 Hz.

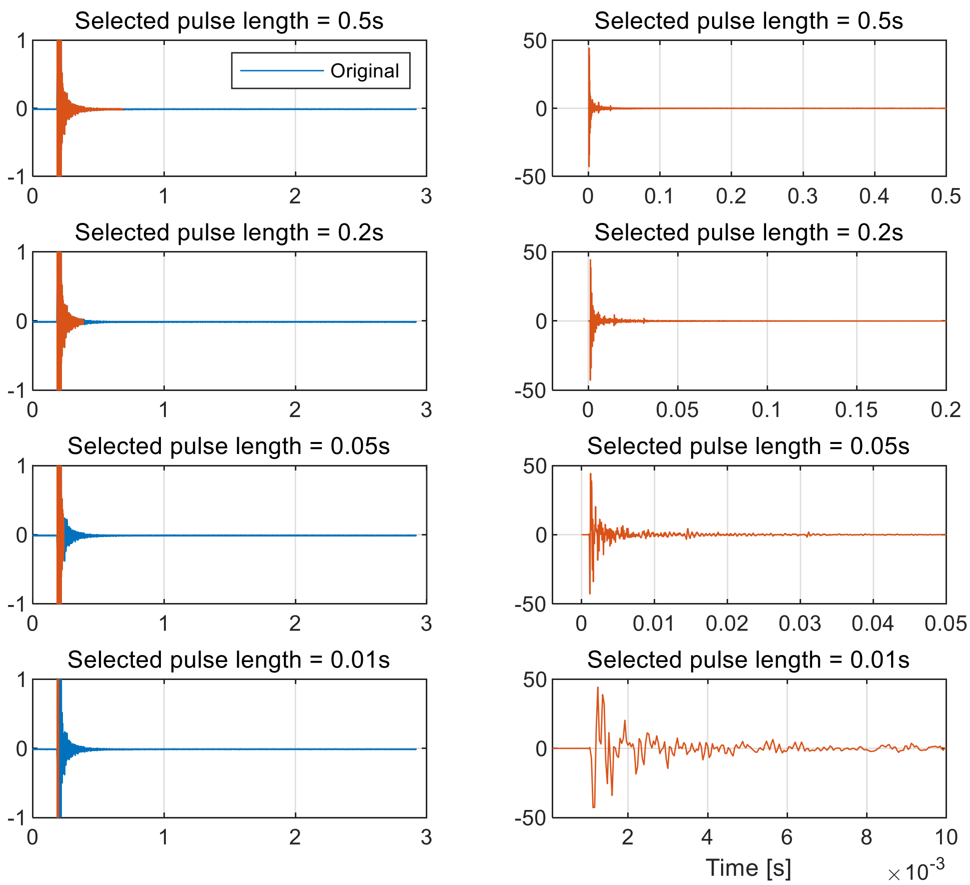


**Figure 5.** Pulse with different duration. **Left**: Y-zoom of selected pulse plotted with full-length pulse as reference, **right**: selected pulse in full scale (note: variable time scale).

The applicability of individual pulses is verified by the shape of their amplitude–frequency characteristics of the approximated frequency response function. From each shortened version of the base pulse, a corresponding full-resolution, one-sided, scaled spectrum is plotted.

Figure 6 shows spectra for five different duration times of pulses: 2 s, 1 s, 0.2 s, 0.05 s, and 0.01 s, which correspond to full resolutions equal to 2 Hz, 5 Hz, 20 Hz, and 100 Hz, respectively. As shown, for all investigated duration times, the amplitude–frequency characteristics show similar dominant resonant frequencies of the structure, which are ca. 1.7–2 kHz and 5–8 kHz. This means that the presented technique enables the modelling of faulty REB signals, for which the characteristic frequencies (ball-passing frequency of the outer race (BPFO), ball-passing frequency of the inner race (BPFI), fundamental train frequency (FTF), and ball spin frequency (BSF)) are all in the range 1–100 Hz.

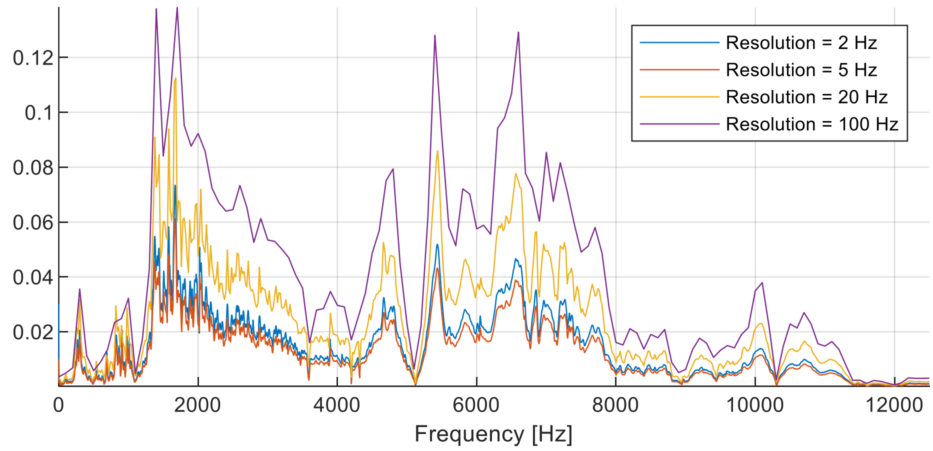


**Figure 6.** Spectrum of pulses with different length (Y-axis manually scaled).

After initial selection and verification, a single base pulse was selected. This pulse is shown in full-scale in Figure 7, and in a zoomed version in Figure 8. This step is referred to as Stage 1 in Figure 1. The base pulse was used in two ways. During the construction of the hybrid vibration signal, individual pulses were generated from the SHORTENED base pulse, taking into account the duration of each consecutive pulse. Next, the FULL LENGTH pulse was used to generate high-resolution amplitude–frequency characteristics, followed by calculations of the instantaneous amplitude of pulses on the basis of machine instantaneous speed.

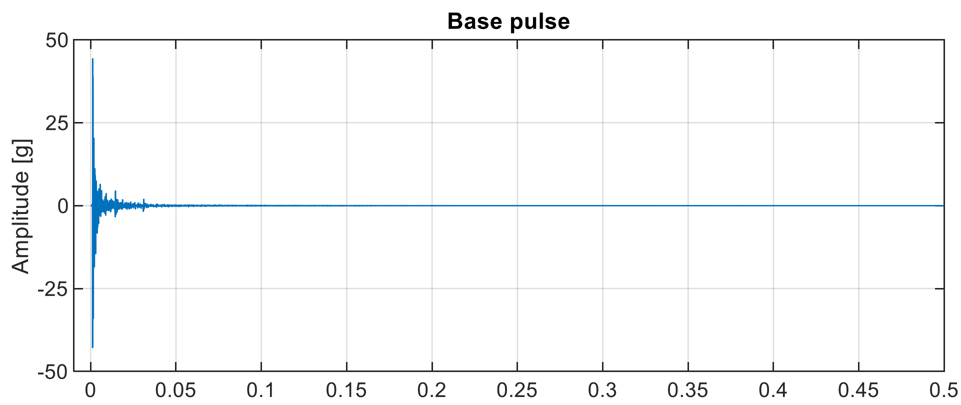


**Figure 7.** Full-scale base pulse.

The base pulse illustrated in Figures 7 and 8 reaches roughly ±50 [g] in amplitude, with the no. of unique points exceeding 5.6 k values (for a 24-bit ADC data acquisition unit (in MATLAB, use length(unique(x)), where x represents the pulse raw waveform)).

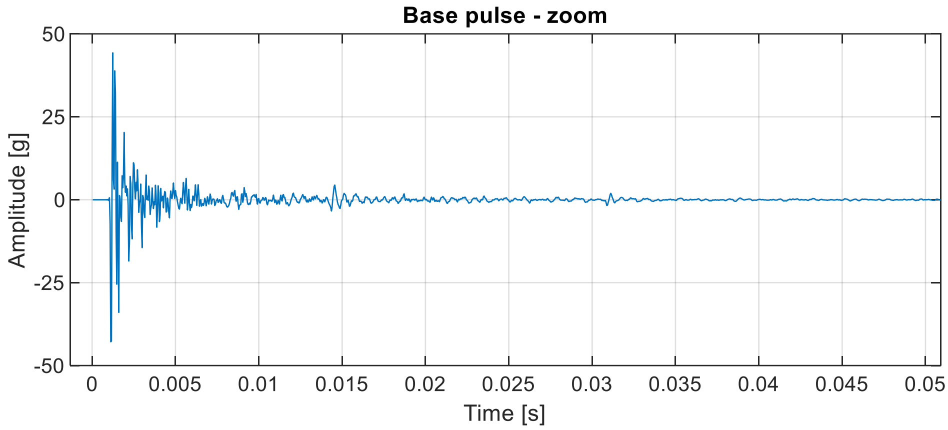


**Figure 8.** Base pulse—zoom.

In the studied example, the signal is modelled with sampling frequency 25 kHz and duration 0.5 s.

### *2.3. Generalized Frequency Modulation*

The method presented in this paper is oriented toward modeling signals of non-stationary machine operational conditions, which requires instantaneous speed data as input, such as the one presented in Figure 9. Machine speed profiles can be synthetically generated [24], or they can be extracted from machine process data with additional up-sampling.

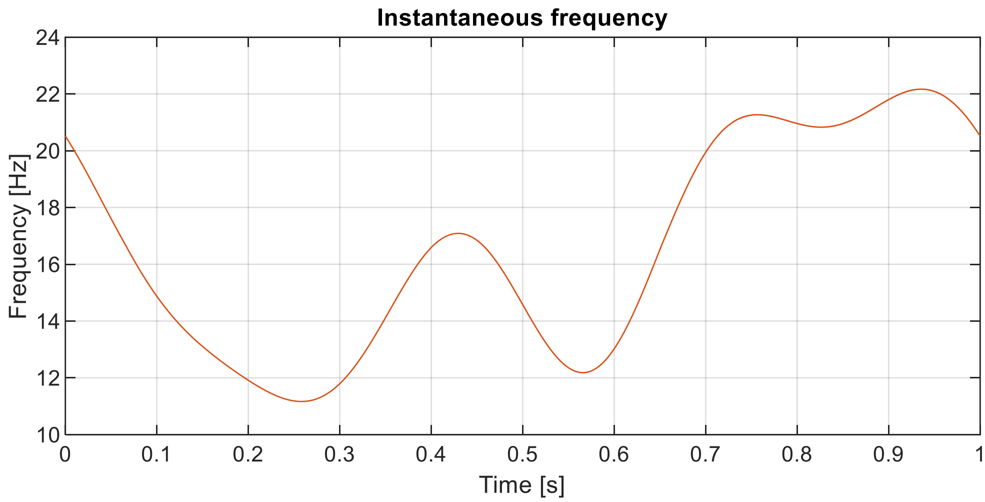


**Figure 9.** Instantaneous frequency profile simulating machine operational speed.

The nominal speed selected was 1000 RPM (rotations per minute), which is ca. 16.667 Hz. In the studied example, the arbitrary speed fluctuation was selected to be +/−5.5 Hz (referred to as "*FM_factor*"). The characteristic bearing BPFO order was arbitrarily selected to be equal to 4.88 (data coming from the author's experience in industry), which results in the nominal frequency of pulses equal to 81.33 Hz. Taking into account the machine instantaneous speed data, and the nominal frequency of bearing pulses, the instantaneous frequency of pulses is calculated, and illustrated in Figure 10.

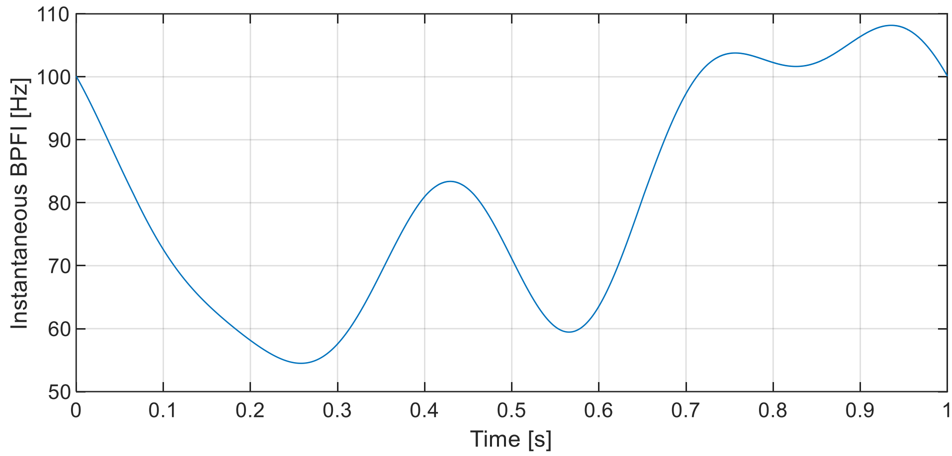


**Figure 10.** Instantaneous frequency of REB pulses.

For each pulse in the signal, the time of the pulse was calculated taking the base pulse and trimming it to the duration corresponding to instantaneous frequency of this pulse. Additionally, bearing jitter was selected to be 2% [25], and added to the signal. The subsequent pulses were concentrated. This step is referred as Stage 2 in Figure 1. Figure 11 illustrates the constant amplitude pulses generated from the base pulse, the duration of which are a function of the machine instantaneous speed.

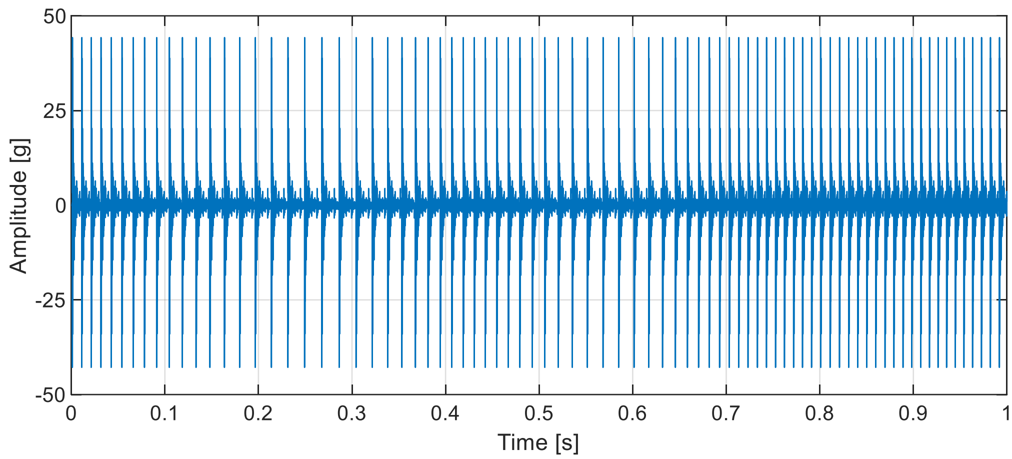


**Figure 11.** Variable-speed pulses.

In next step, the amplitude of the pulses were modified.

### *2.4. Generalized Amplitude Modulation*

The amplitude of individual pulses were scaled according to the amplitude–frequency characteristics of the frequency response function of the object and the machine operational speed, as illustrated in Figure 12. For the considered machine, the speed oscillates in the range of 11–22 Hz, so only this range of amplitude–frequency characteristics of simplified frequency response function (FRF) is of interest. As the resolution of this characteristic is 2 Hz (due to 0.5 s pulse length), there are only 7 points in the 11–22 Hz range. On the other hand, the resolution of the instantaneous speed is much higher (25,000 pints). For this reason, a large portion of FRF profile data needed to be interpolated [24].

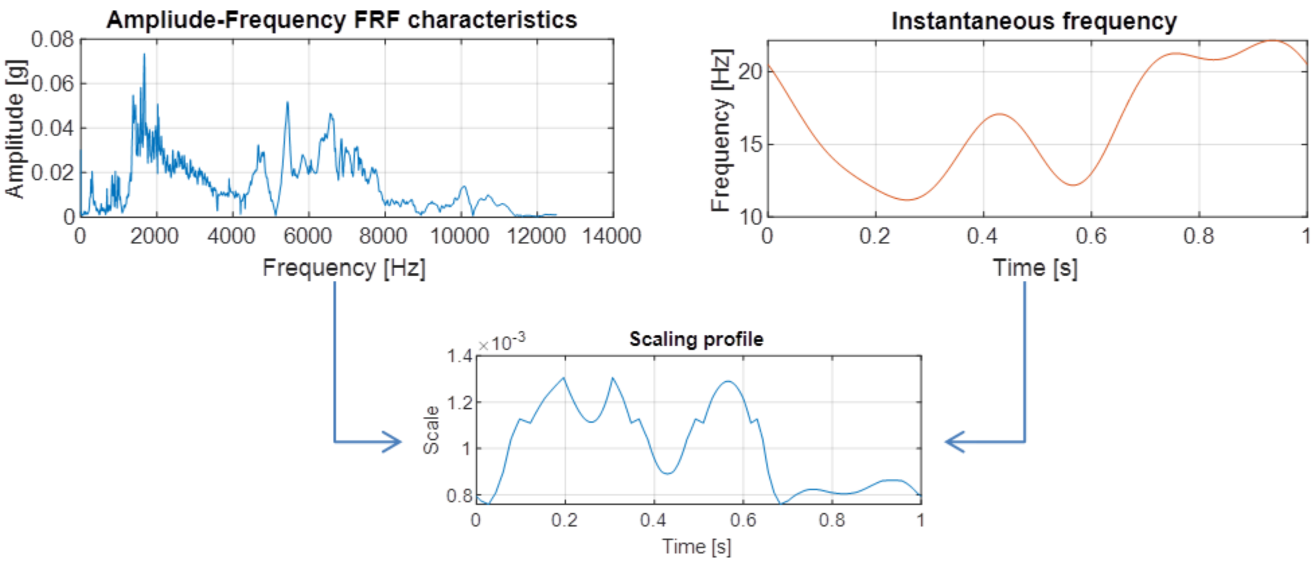


**Figure 12.** Calculation of amplitude of pulses.

Generally, the presented scaling methodology represents the change in power of the vibration signal generated by a rotary machinery as its speed changes. In particular, the scaling signal amplitude, as a function of instantaneous frequency data, and the FRF profile represent variable input forces of the system, which result in the variable system response for the time-invariant FRF.

### 2.5. Resultant Hybrid Signal

Figure 13 represents resultant hybrid vibration signal and corresponding machine instantaneous speed. As observed, frequency of pulses changes proportionally to the speed, which results in frequency signal modulation (FM). Simultaneously, the amplitude of pulses changes as a function of speed and FRF, resulting in profiled amplitude modulation (AM). For this reason, such data is classified as a generalized AM–FM signal.

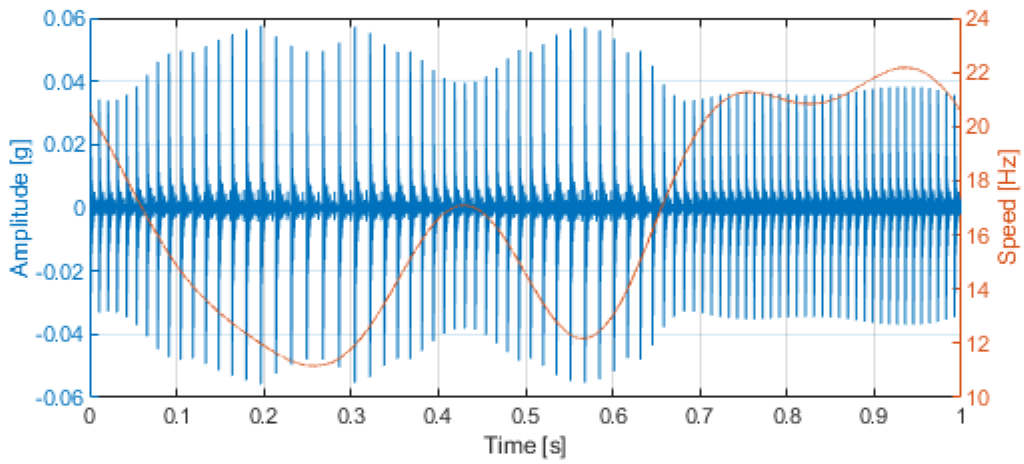


**Figure 13.** Resultant REB signal with instantaneous speed profile.

The data presented in Figure 13 corresponds to Stage 3 in Figure 1. The following part of the paper shows spectral analysis of the generated hybrid signal.

## 3. Signal Analysis

### *3.1. Frequency Domain Analysis*

#### 3.1.1. Full-Resolution Spectrum

Section 2 demonstrates the methodology of the generation of hybrid vibration signal representing an REB local fault in a regime of highly non-stationary operational conditions. The current section demonstrates spectral analysis of this signal, which is used to verify the methodology. Figure 14 illustrates the full-resolution spectrum of the generated signal. As a reference, the plot contains a spectral mask, which is generated from a single base pulse, trimmed to the average pulse length in the signal, which is:

$$\frac{No.pulses}{\sum REB\_inst.freq_i} = 0.0123[\mathrm{s}]$$

From this length, the spectral resolution of the amplitude–frequency characteristics of the FRF profile is equal to:

$$ceil\left(\frac{\sum REB_{inst}.freq_i}{No.pulses}\right) = 82\ \mathrm{Hz}$$

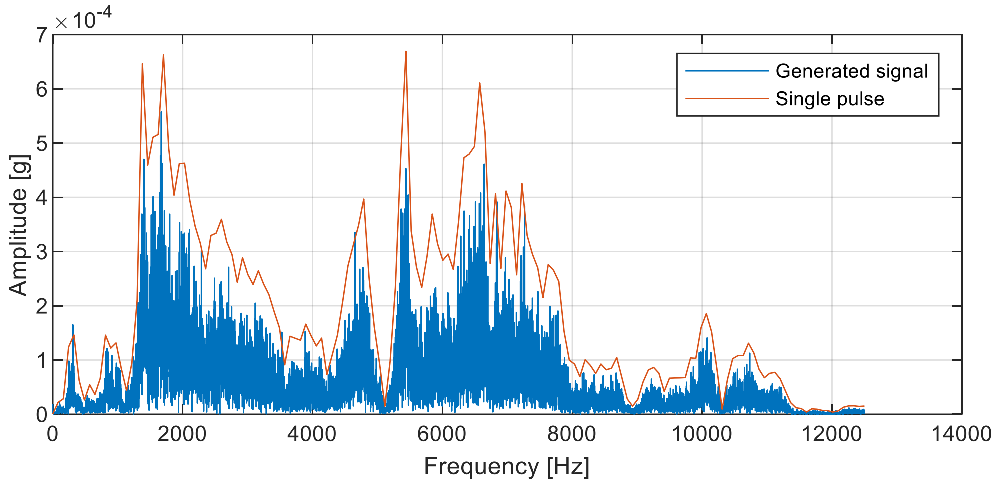


**Figure 14.** Full-resolution spectrum of generated vibration signals.

The referential spectrum is noted in Figure 14 as "Single pulse" data. As illustrated in Figure 14, the full-resolution spectrum of the hybrid generated signal is accurately mapped by a spectral mask generated from the real, single base pulse. Next, the envelope time waveform and envelope spectrum of the generated signal are calculated.

#### 3.1.2. Envelope Analysis (In Frequency Domain)

For envelope analysis in the frequency domain, typical parameters are accepted, i.e., an HP cutoff frequency equal to 2000 Hz, and an LP cutoff frequency equal to 500 Hz. It is worth mentioning that the constructed signal does not contain low-frequency deterministic components, so the HP filtering is of secondary importance. Figure 15 illustrates the corresponding envelope time waveforms and envelope spectrum.

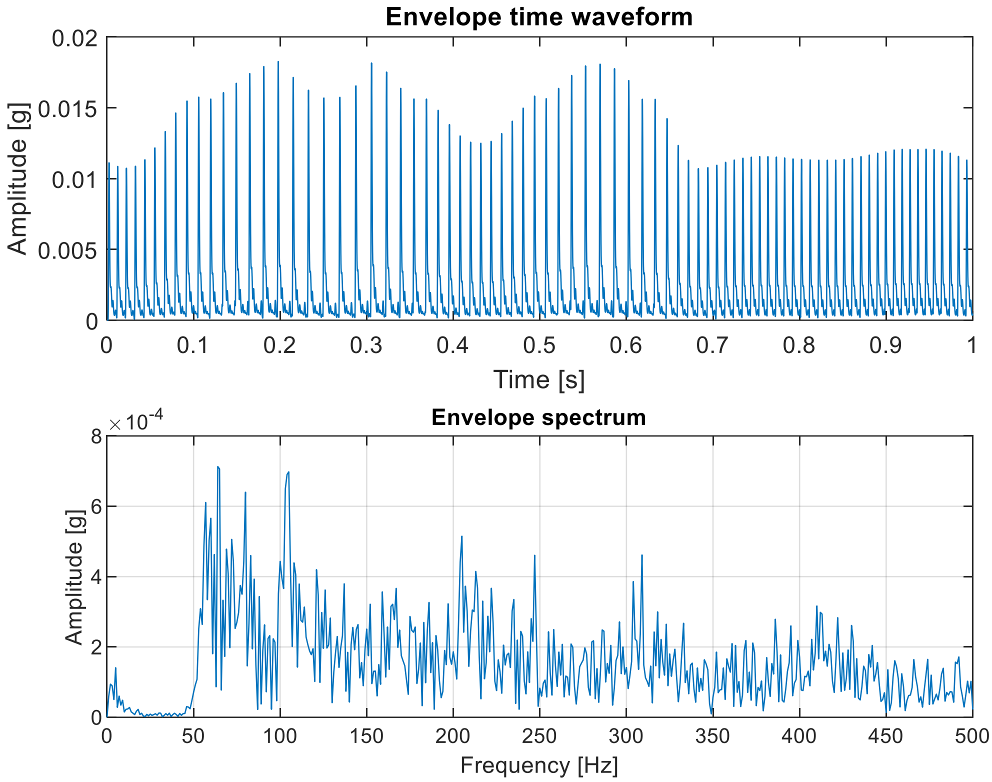


**Figure 15.** Envelope analysis of the generated signal in the frequency domain.

As observed in Figure 15, the envelope spectrum does not indicate the presence of REB characteristic components, clearly seen in the corresponding time-domain waveform as a cyclo-non-stationary signal [23]. This result comes from the relatively large speed fluctuation of the signal, roughly: $((22 - 12\ \text{Hz})/16{,}667\ \text{Hz}) * 100\% = 60\%$. In order to solve the problem of spectral smearing of the envelope signals, the calculations are repeated in the angle/order domains.

### *3.2. Angle-Domain Analysis*

#### 3.2.1. Phase Marker Generation

Although the presented hybrid signal is constructed using a smooth instantaneous profile, the model only covers pulses composed of random, multi-band carrier frequencies, not individually affected by variable speed. In other words, individual pulses are modelled as subsequent non-stationary time-invariant systems in a time-variant regime [26], resulting (as mentioned earlier) in a cyclo-non-stationary signal. Thus, it is possible to generate the phase marker (PM) signal by concentrating binary segments [1 0 0 0 . . . 0] for every consecutive pulse, where 1 represents the start of the pulse, and is then zero-padded to the length equal to the length of the current pulse. Such a technique additionally generates PM signal, which is unaffected by REB jitter, and, thus, is more accurate. Figure 16 illustrates a generated PM signal mapped on the AM–FM REB signal in this way.

As illustrated in Figure 16, the accepted method for PM generation results in the perfect mapping of the instantaneous frequency modulation of REB-generated pulses. However, in this scenario, the nominal time resolution of the PM signal is equal to the reciprocal of the REB characteristic frequency, which could be inconvenient, because in a typical industrial scenario, PM gives one pulse per shaft rotation (here 16.667 Hz). For comparative analysis, Section 3.2.2 illustrates the post-generation of PM signal (so-called PM reconstruction), while the following Section 3.2.3 shows the difference between both approaches, i.e., when the phase marker is pre-generated, and when it is reconstructed.

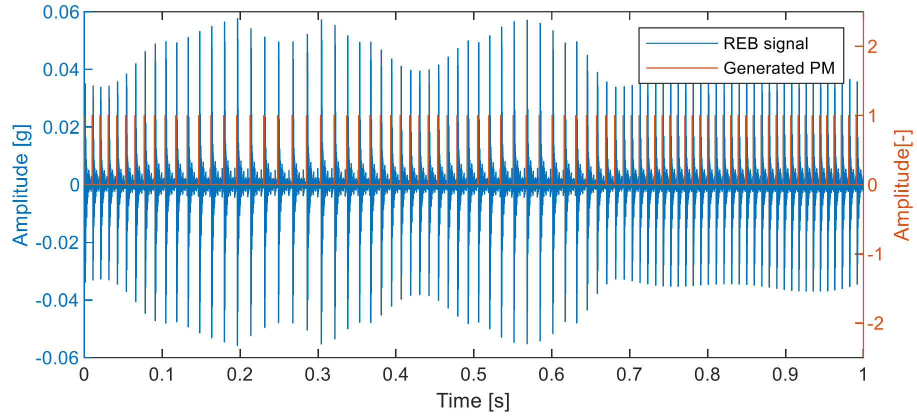


**Figure 16.** Generated phase marker signal.

3.2.2. Phase Marker Reconstruction

Although many specialized speed recovery methods exist [27,28], they generally require the presence of a deterministic phase-locked component in the signal, so they are not suitable for the considered case. Therefore, the phase marker data is recovered from a pre-generated FM sinusoidal component in a plain way. Such PM data is generated in two steps. Firstly, a frequency-modulated representative sinusoidal component is generated independently. Secondly, the number of times of subsequent zero-crossing of this component are evaluated. Each time is determined when two conditions are met, namely, when consecutive data have a lower amplitude than previous data, and experience signs change from negative to positive. In the considered case, two cases, represented by Formulas (3) and (4), are possible (see Section 2.3. for definition of *FM_factor*):

$$PM_{shaft} = \sin(2\pi\cdot(\frac{1000}{60}\cdot t + 2\pi\cdot FM\_factor \int inst.frequency\cdot dt)) \tag{3}$$

$$PM_{REB} = \sin(2\pi\cdot(\frac{1000}{60}\cdot BPFO\cdot t + 2\pi\cdot FM\_factor\cdot BPFO \int inst.frequency\cdot dt)) \tag{4}$$

Formula (3) corresponds to the PM signal recovered from the frequency-modulated shaft component, i.e., machine instantaneous speed, while Formula (4) corresponds to the instantaneous frequency of REB characteristic components, BPFO. Figure 17 illustrates the presented idea for the *PM_shaft* version.

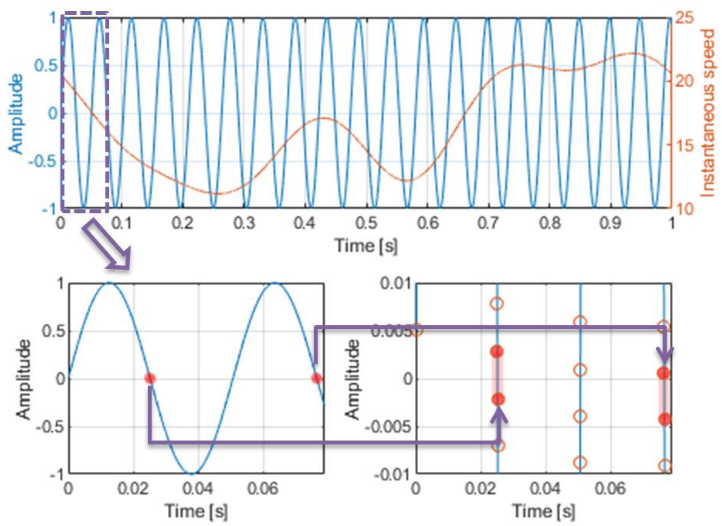


**Figure 17.** The concept of PM data recovery. **Top**: machine instantaneous speed component. **Bottom left**: first full rotation. **Bottom right**: data points used in PM calculations.

Two bottom subplots in Figure 17 illustrate the data corresponding to the first full rotation. The right subplot shows four precise points, which fulfill the abovementioned condition; therefore, they constitute a single PM entry. Subsequent PM data is calculated in the same way, resulting in binary PM 1D (one dimensional) data. The resultant PM signal is plotted in Figure 18. In the case of the REB-reconstructed PM, the results are analogous. Section 3.2.3 addresses the performance of the presented method.

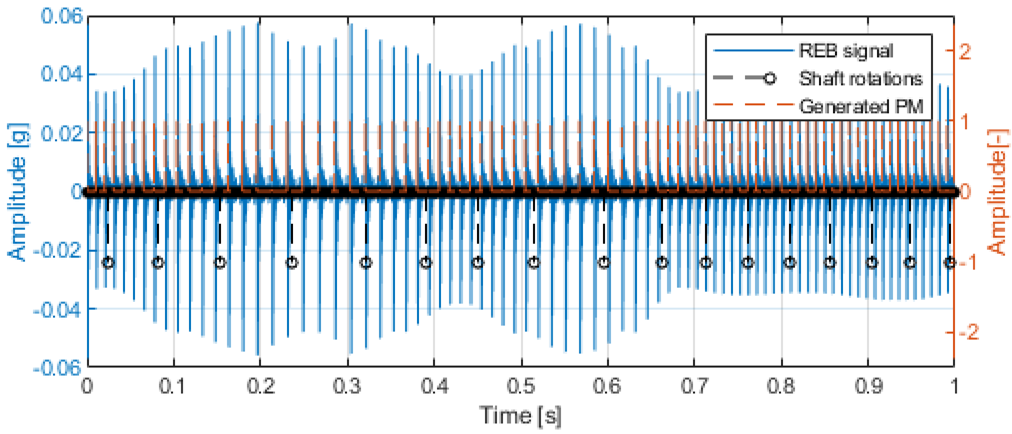


**Figure 18.** PM signal reconstructed from shaft component.

### 3.2.3. Comparison of Pre-Generated and Reconstructed Phase Marker Signal

Figure 19 shows the comparison of three different phase marker signals: the PM signal reconstructed from the shaft component (16 points) compared with shaft instantaneous speed (25 k points), and the PM signal reconstructed from the REB component (80 points) compared with REB component instantaneous speed (25 k points), along with the PM signal pre-generated simultaneously with the REB vibration signal.

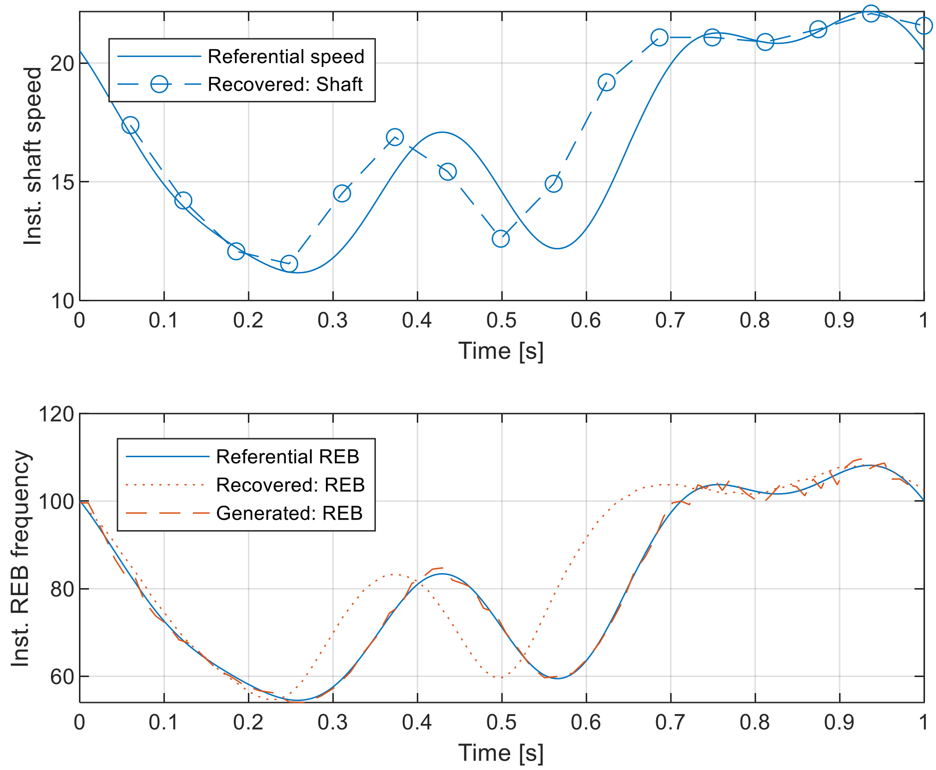


**Figure 19.** Comparison of different PM signals.

As observed in Figure 19, the pre-generated PM signal is the only PM signal that actually perfectly matches the timestamps of individual pulses, which is endorsed by PM lot-mapped on the hybrid vibration signal shown in Figure 18. The above study illustrates a general problem with the resampling of vibration signals containing cyclo-non-stationary components with additional jitter; the transformation into the angle domain on the basis of instantaneous frequency of deterministic components introduces errors during interpolation.

#### 3.2.4. Resampling

As indicated in Section 3.2.3, the pre-generated PM signal is most suitable for the resampling of the hybrid cyclo-non-stationary component from the three investigated methods. The resampled signal presents pulse responses equally spaced in the angle domain, as illustrated in Figure 20.

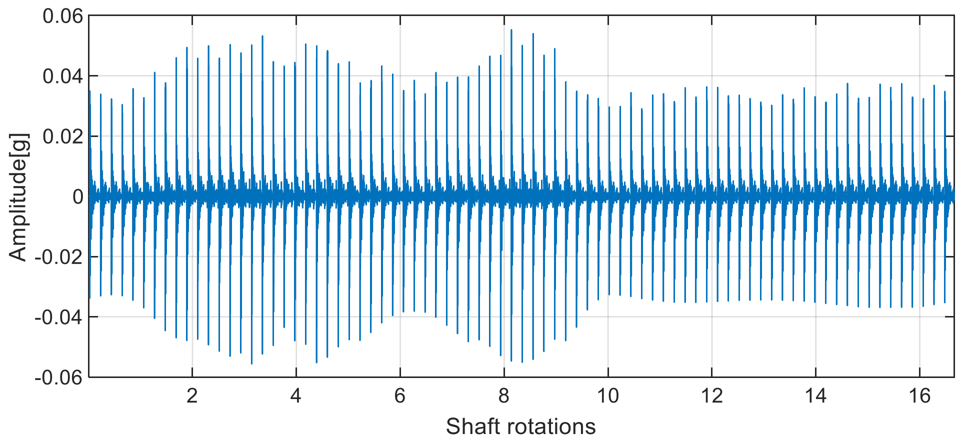


**Figure 20.** REB signal in angle domain with reference to shaft rotations.

Taking into account that the input instantaneous speed profile simulated shaft instantaneous speed, the angle axis (display clarity) in Figure 20 is re-scaled from REB characteristic frequency to shaft characteristic frequency

#### 3.2.5. Envelope Order Spectrum Analysis

In order to preserve the envelope settings accepted in Section 3.1.2, i.e., envelope analysis in the frequency domain, the corresponding cut-off values in the order domain are as follows:

**Shaft-recovered PM**

HP_cutoff = 2000 Hz/shaft_nominal_speed [Hz]
LP_cutoff = 2000 Hz/shaft_nominal_speed [Hz]

**REB-recovered PM**

HP_cutoff = 2000 Hz/shaft_nominal_speed [Hz]/REB_characteristic_order
LP_cutoff = 2000 Hz/shaft_nominal_speed [Hz]/REB_characteristic_order

**REB-pre-generated PM**

HP_cutoff = 2000 Hz/shaft_nominal_speed [Hz]/REB_characteristic_order
LP_cutoff = 2000 Hz/shaft_nominal_speed [Hz]/REB_characteristic_order

The envelope order spectra in full order resolution for considered resampled signals are illustrated in Figure 21. For clarity, the order scale of spectra calculated using REB-recovered PM and REB-pre-generated PM are re-scaled to shaft orders. As indicated by Figure 21, the only envelope order spectrum that does not experience spectral smearing is the envelope spectrum calculated from the signal resampled using pre-generated PM data.

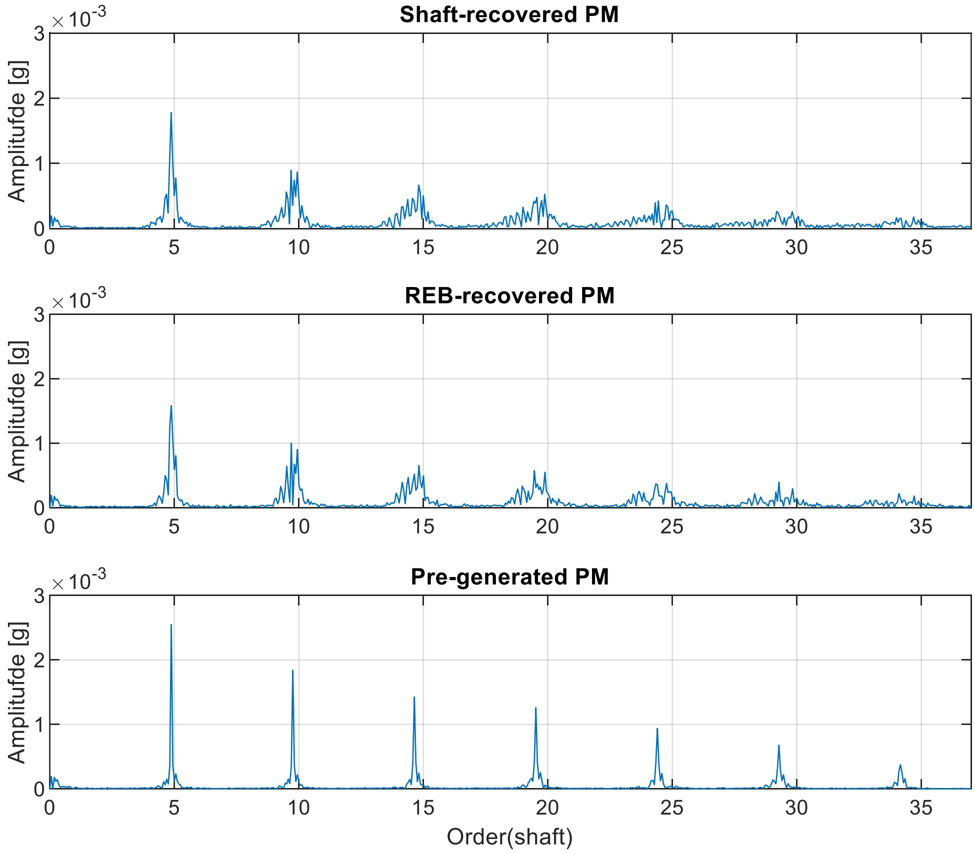


**Figure 21.** Envelope order spectra.

In case of signals resampled with respect to recovered PM data, both shaft-recovered and REB-recovered spectral components in the envelope order spectrum are clearly smeared, which is detrimental for the order analysis of the vibration signal. For this reason, it could be accepted that the presented methodology is suitable for the generation of a hybrid cyclo-non-stationary signal component.

## 4. Conclusions

The presented technique shows the concept of a hybrid model of vibration signal generated by a faulty rolling-element bearing. The model uses real pulse response data for two purposes; namely, as a base pulse, and as an amplitude ratio profile calculated from the amplitude–frequency characteristics of the frequency response function of the structure. The instantaneous machine speed data are used as a separate input entry, and this can be real historical data, or a smooth simulated profile. The presented model is verified for signals of length 1–10 s, sampling frequency 25 kHz, and a rolling-element bearing nominal characteristic frequency from 10 Hz to 100 Hz. Due to its hybrid nature, and the simplicity of generation, the presented model serves as an attractive alternative to other physical or data-driven models from the literature discussed in the paper. The proposed method enables the generation of vibration signals corresponding to defects of the real selected bearing mounted on the machinery, without constructing its physical model, and without collecting data from individual failure modes. Finally, the paper shows that the methods of analysis of cyclo-nonstationary signal components, such as those generated by a faulty REB, could perform better if these components are treated as individual, consecutive, time-invariant signal fragments under a global time-variant regime.

**Funding:** This research was funded by The National Centre for Research and Development (NCBR), grant number POIR.04.01.04-00-0080/19-00.

**Institutional Review Board Statement:** Not applicable.

**Informed Consent Statement:** Not applicable.

**Data Availability Statement:** Not applicable.

**Conflicts of Interest:** The author declares no conflict of interest.

## References

1. Gebraeel, N.; Lawley, M.; Liu, R.; Parmeshwaran, V. Residual Life Predictions from Vibration-Based Degradation Signals: A Neural Network Approach. *IEEE Trans. Ind. Electron.* **2004**, *51*, 694–700. [CrossRef]
2. Concli, F.; Cortese, L.; Vidoni, R.; Nalli, F.; Carabin, G. A mixed FEM and lumped-parameter dynamic model for evaluating the modal properties of planetary gearboxes. *J. Mech. Sci. Technol.* **2018**, *32*, 3047–3056. [CrossRef]
3. Zghal, B.; Graja, O.; Dziedziech, K.; Chaari, F.; Jablonski, A.; Barszcz, T.; Haddar, M. A new modeling of planetary gear set to predict modulation phenomenon. *Mech. Syst. Signal Process.* **2019**, *127*, 234–261. [CrossRef]
4. Jin, X.; Que, Z.; Sun, Y.; Guo, Y.; Qiao, W. A Data-Driven Approach for Bearing Fault Prognostics. *IEEE Trans. Ind. Appl.* **2019**, *55*, 3394–3401. [CrossRef]
5. Wang, Y.; Peng, Y.; Zi, Y.; Jin, X.; Tsui, K.-L. A Two-Stage Data-Driven-Based Prognostic Approach for Bearing Degradation Problem. *IEEE Trans. Ind. Inform.* **2016**, *12*, 924–932. [CrossRef]
6. Leturiondo, U.; Mishra, M.; Galar, D.; Salgado, O. Synthetic data generation in hybrid modelling of rolling element bearings. *Insight-Non-Destr. Test. Cond. Monit.* **2015**, *57*, 395–400. [CrossRef]
7. Sunnersjo, C.S. Varying compliance vibrations of rolling element bearings. *J. Sound Vib.* **1978**, *58*, 363–373. [CrossRef]
8. McFadden, P.D.; Smith, J.D. Model for the vibration produced by a single point defect in a rolling element bearing. *J. Sound Vib.* **1984**, *96*, 69–82. [CrossRef]
9. McFadden, P.D.; Smith, J.D. The vibration produced by multiple point defect in a rolling element bearing. *J. Sound Vib.* **1985**, *98*, 263–273. [CrossRef]
10. Su, Y.T.; Lin, M.H.; Lee, M.S. The Effects of Surface Irregularities on Roller Bearing Vibrations. *J. Sound Vib.* **1999**, *165*, 455–466. [CrossRef]
11. Ahmadi, A.M.; Howard, C.Q.; Peterson, D. The path of rolling elements in defective bearings: Observations, analysis and methods to estimate spall size. *J. Sound Vib.* **2016**, *366*, 277–292. [CrossRef]
12. Mishra, C.; Samantaray, A.K.; Chakraborty, G. Ball bearing defect models: A study of simulated and experimental fault signatures. *J. Sound Vib.* **2017**, *400*, 86–112. [CrossRef]
13. Wrzochal, M.; Adamczak, S. The problems of mathematical modelling of rolling bearing vibrations. *Bull. Pol. Acad. Sci. Tech. Sci.* **2020**, *68*, 1363–1372.
14. Wang, Z.; Zhu, C. A new model for analyzing the vibration behaviors of rotor-bearing system. *Commun. Nonlinear Sci. Numer. Simul.* **2019**, *83*, 105130. [CrossRef]
15. Sunnersjo, S. Rolling Bearing Vibrations: The Effects of Geometrical Imperfections and Wear. *J. Sound Vib.* **1985**, *98*, 455–474. [CrossRef]
16. Wardle, F.P. Vibration forces produced by waviness of the rolling surfaces of thrust loaded ball bearings Part 2: Experimental validation. *Proc. Inst. Mech. Eng. Part C J. Mech. Eng. Sci.* **1988**, *202*, 313–319. [CrossRef]
17. Aschenbrenner, A.; Schleich, B.; Tremmel, S.; Wartzack, S. A variational simulation framework for the analysis of load distribution and radial displacement of cylindrical roller bearings. *Mech. Mach. Theory* **2020**, *147*, 103769. [CrossRef]
18. Tarelko, W. Methods of building dynamical system models in mechanics. *Mechanik* **2015**, *10*, 834. [CrossRef]
19. Borghesani, P.; Smith, W.; Randall, R.; Antoni, J.; El Badaoui, M.; Peng, Z. Bearing signal models and their effect on bearing diagnostics. *Mech. Syst. Signal Process.* **2022**, *174*, 109077. [CrossRef]
20. Borghesani, P.; Ricci, R.; Chatterton, S.; Pennacchi, P. A new procedure for using envelope analysis for rolling element bearing diagnostics in variable operating conditions. *Mech. Syst. Signal Process.* **2013**, *38*, 23–35. [CrossRef]
21. Randall, R.B. *Vibration-Based Condition Monitoring: Industrial, Aerospace and Automotive Applications*; John Wiley & Sons: Hoboken, NJ, USA, 2011.
22. Antoni, J. Cyclostationarity by examples. *Mech. Syst. Signal Process.* **2009**, *23*, 987–1036. [CrossRef]
23. Abboud, D.; Baudin, S.; Antoni, J.; Rémond, D.; Eltabach, M.; Sauvage, O. The spectral analysis of cyclo-non-stationary signals. *Mech. Syst. Signal Process.* **2016**, *75*, 280–300. [CrossRef]
24. Jablonski, A. *Condition Monitoring Algorithms in MATLAB*; Springer: Berlin/Heidelberg, Germany, 2021.
25. Randall, R.B. The relationship between spectral correlation and envelope analysis in the diagnostics of bearing faults and other cyclostationary machine signals. *Mech. Syst. Signal Process.* **2001**, *15*, 945–962. [CrossRef]
26. Dziedziech, K.; Staszewski, W. Wavelet-based transmissibility for the analysis of time-variant systems. *Mech. Syst. Signal Process.* **2020**, *145*, 106918. [CrossRef]

27. Dziedziech, K.; Jablonski, A.; Dworakowski, Z. A novel method for speed recovery from vibration signal under highly non-stationary conditions. *Measurement* **2018**, *128*, 13–22. [CrossRef]
28. Urbanek, J.; Barszcz, T.; Antoni, J. A Two-Step Procedure for Estimation of Instantaneous Rotational Speed with Large Fluctuations. *Mech. Syst. Signal Process.* **2013**, *38*, 96–102. [CrossRef]